Journal of Volcanology and Geothermal Research 344 (2017) 185–196

Contents lists available at ScienceDirect

Journal of Volcanology and Geothermal Research

journal homepage: www.elsevier.com/locate/jvolgeores

Time-dependent Coulomb stress changes induced by the 2002–2003 Etna magmatic intrusions and implications on following seismic activities

Fabio Pulvirenti [a], Marco Aloisi [b,*], Shuanggen Jin [a,c]

[a] Shanghai Astronomical Observatory, Chinese Academy of Sciences, Shanghai, China
[b] Istituto Nazionale di Geofisica e Vulcanologia, Osservatorio Etneo, Catania, Italy
[c] Department of Geomatics Engineering, Bulent Ecevit University, Zonguldak 67100, Turkey

ARTICLE INFO

Article history:
Received 6 April 2016
Received in revised form 7 October 2016
Accepted 2 November 2016
Available online 5 November 2016

Keywords:
Coulomb stress changes
Finite element model
Viscoelasticity
Earthquakes
Mount Etna

ABSTRACT

In this paper, the relationship between the dike-forming magmatic intrusions and the faulting process at Mount Etna is investigated in terms of Coulomb stress changes. As case study, a complete time-dependent 3-D finite element model for the 2002–2003 eruption at Mount Etna is presented. In the model, which takes into account the topography, medium heterogeneities and principal fault systems in a viscoelastic/plastic rheology, we sequentially activated three dike-forming processes and looked at the induced temporal evolution of the Coulomb stress changes, during the co-intrusive and post-intrusive periods, on Pernicana and Santa Venerina faults. We investigated where and when fault slips were encouraged or not, and consequently how earthquakes may have been triggered. Results show positive Coulomb stress changes for the Pernicana Fault in accordance to the time, location and depth of the 27th October 2002 Pernicana earthquake ($M_d = 3.5$). The amount of Coulomb stress changes in the area of Santa Venerina Fault, as induced by dike-forming intrusions only, is instead almost negligible and, probably, not sufficient to trigger the 29th October Santa Venerina earthquake ($M_d = 4.4$), occurred two days after the start of the eruption. The necessary Coulomb stress change value to trigger this earthquake is instead reached if we consider it as induced by the 27th October Pernicana biggest earthquake, combined with the dike-induced stresses.

1. Introduction

One of the most challenging problems in studying the tectonic deformations is to understand the conditions under which rock fails along the fault planes and how the fault movements are related each other. These relationships can be investigated by the estimated stress changes along the faults before and after the earthquakes. At Mount Etna, the stress, triggered by the push of the dike-forming intrusions, together with the regional compressive regime, is transferred to the faults and redistributed among them (e.g., Patanè et al., 2005; Feuillet et al., 2006; Mattia et al., 2007; Currenti et al., 2008a; Aloisi et al., 2011; Bonanno et al., 2011; Privitera et al., 2012; Gonzalez and Palano, 2014). In particular, Feuillet et al. (2006), after analyzing historical earthquakes in eastern Sicily and eruptions at Mt. Etna volcano, clearly found that volcanic sources and active faults, located nearby the volcano, are mechanically coupled, and therefore they can interact each other by changing or perturbing the stress state and, in turn, promoting or inhibiting earthquakes or eruptions.

If earthquakes occur, the stress state of the medium is modified by an additional stress field (e.g., Dragoni et al., 1982; Privitera et al., 2012). The stress changes depend on fault location, geometry and sense of slip (rake). It is commonly referred to stress changes as Coulomb stress changes, hereafter CSC. The importance of the CSC in imaging the areas of stress transfer among faults has been widely demonstrated in many works (e.g., Thatcher and Savage, 1982; Harris and Simpson, 1992; Jaumé and Sykes, 1992; Reasenberg and Simpson, 1992; King et al., 1994; Gross and Kisslinger, 1997; Harris, 1998; Nostro et al., 1998; Vidale et al., 1998; Stein, 1999; Hill et al., 2002; Marzocchi et al., 2002; Toda et al., 2002; Hyodo and Hirahara, 2004; Walter and Amelung, 2004; Feuillet et al., 2006; Calais et al., 2010; Toda et al., 2011). The estimated stress increases are rarely more than a few bars (1 bar, which is approximately atmospheric pressure at sea level), or just a few percent of the mean earthquake stress drop (Stein, 1999). The CSC quantity (bar) can be regarded as an alteration of the "potentiality" of slip of the fault plane in response to the current stress state of the medium (Kilb et al., 2000). If this quantity is positive (or negative), the movement on the fault plane is encouraged (or

* Corresponding author.
E-mail addresses: fabiopulvirenti@yahoo.it (F. Pulvirenti), marco.aloisi@ingv.it (M. Aloisi), sgjin@shao.ac.cn (S. Jin).

http://dx.doi.org/10.1016/j.jvolgeores.2016.11.001
0377-0273/

discouraged) and earthquakes can be generated (or not). Incorporating, as we here made, the viscoelastic effects that modify the Coulomb stress with time, the variation of the stress changes in space and time through the lithosphere can give information on the arrival of a "stress wave" (e.g., Pollitz and Sacks, 1997; Freed and Lin, 1998; Kenner and Segall, 1999; Sevilgen et al., 2012) on a seismogenetic structure, this "wave" might then trigger an earthquake in this zone, if the right conditions (depending on rheology, friction and connection between crustal discontinuities) are found. Moreover, the stress distribution among the faults can be used to investigate the relation between the mainshock on a fault and the probability of aftershocks in the nearby faults. The strong concentration of aftershocks found at the site of such small stress increases is explained in terms of rupture nucleation phenomena, observed in laboratory (Stein, 1999).

The minimum positive value of CSC to trigger an earthquake depends on the area where the fault is located because of the different rheological conditions. In the Etnean area, changes much lower than 1 bar are considered usually sufficient to trigger movements on the fault plane (Bonanno et al., 2011; Privitera et al., 2012; Gonzalez and Palano, 2014). In some areas, aftershocks can be triggered even when the stress is increased by about 0.3 bar (Toda et al., 2011). Many authors (e.g., Harris and Simpson, 1992; Jaumé and Sykes, 1992; Reasenberg and Simpson, 1992; Gross and Kisslinger, 1997; Stein, 1999; Bonanno et al., 2011; Privitera et al., 2012) reported that static stress changes greater than or equal to 0.1 (bar) may trigger seismicity within a rock volume, close to the critical state of failure. For example, it was found that 67% of the 10,000 M > 1 Landers (California, 1992, $M_w = 7.3$) aftershocks occurred in regions calculated to have been brought >0.1 bar closer to failure and few aftershocks occurred in regions inhibited by >0.1 bar from failure (stress shadows), (Stein, 1999). Anderson and Johnson (1999) obtained that aftershocks of the 1987 ($M_w = 6.6$) sequence at Superstition Hills (California) show significant correlations for stress increases >0.1 bar during 1.4–2.8 yr after the mainshock. An earthquake, producing weak stress increases, can thus enhance or suppress subsequent events, depending on their location and orientation. Viewed in this light, aftershocks are simply sites of seismicity rate increase, occurring where the stress has increased (Stein, 1999). Some authors retain that the CSC lower limit, for a significant correlation between seismicity rate change and static stress changes, could be considered equal to the value produced by tides (about 0.01 bar). In fact, Vidale et al. (1998) found that, along the creeping portions of the San Andreas and Calaveras faults, the rate of seismicity during the peak tidal unclamping is 1.0% higher than average. Thus, even tides can perceptibly alter the rate of seismicity, suggesting that the much larger stress changes associated with earthquakes are indeed one cause of seismicity rate changes. Therefore, a significant lower limit for the CSC can be considered as equal to about 0.1 bar. Moreover, seismic waves (e.g., Stein, 1999; Cai, 2001; Resende et al., 2010; Kamatchi et al., 2013) excited by earthquakes produce dynamic CSC that, at distances more than about one source dimension from the fault, can be an order of magnitude larger than the, here discussed, static stress changes. Since the transient stress oscillate, stress changes are everywhere positive and, therefore, dynamic stresses should produce no seismicity rate decreases, at odds with observations (Stein, 1999). Therefore, exclusively the weak permanent stress changes should control the seismicity. Alternatively, some authors (e.g., Kilb et al., 2000) found that dynamic stresses alter the mechanical state or properties of the fault zone and these dynamically weakened faults may fail after the seismic waves have passed.

In this paper, the relationship between the dike-forming magmatic intrusions and the faulting process at Mount Etna is investigated in terms of static CSC. The model is developed using the commercial software COMSOL Multiphysics (https://www.comsol.com/) and it is an improvement of a previous 3D finite element model (Aloisi et al., 2011). In particular, considering the analysis of the spatial-temporal evolution of the epicentral pattern during the period of 26–29 October 2002 as described in (Barberi et al., 2004) and (Palano et al., 2009), we used the equations described in Piombo et al. (2007) for shear and tensile dislocations in a viscoelastic halfspace, adapting them for heterogeneities, where the viscoelastic areas are described by a generalized Maxwell model. We included also a plastic layer representing the ductile carbonates substrate corresponding to the Hyblean Plateau (Heap et al., 2013; Bakker et al., 2015). It is noteworthy that long-lived magma bodies are present at depths corresponding to the Hyblean Plateau (e.g., Chiarabba et al., 2000) that starts at about a depth of 5 km underneath the volcanic edifice and has an average thickness of about 10 km. Therefore, the involvement of the Hyblean Plateau with the magmatic plumbing system at Mt. Etna volcano, potentially exposes fresh and unaltered carbonate rock to high temperatures (Heap et al., 2013). Thermal-stressing results in a progressive and significant change in the physical properties of the rocks (Heap et al., 2013). Inside this FEM model, we activated sequentially (in a time-dependent manner) each dike-forming process, whose size and position has been evinced by previous calculations (see Aloisi et al., 2011). Since the sequential activation of the dike-forming processes induces a variation in the CSC, which can be monitored with respect to the time (Pollitz and Sacks, 1997; Freed and Lin, 1998; Kenner and Segall, 1999; Toda et al., 2002; Sevilgen et al., 2012), we looked at the temporal effect of the dike-forming intrusions on Pernicana and Santa Venerina faults, which were reactivated during the eruption period. In particular, we looked at the temporal variation of the CSC in relation to two seismic events, the 27th October 2002 01:28 GMT Pernicana earthquake ($M_d = 3.5$) and the 29th October 10:02 GMT Santa Venerina earthquake ($M_d = 4.4$), see Fig. 1. The evolution of the CSC in the eastern flank during the 26–29 October 2002 was investigated through the following two phases: a) in the first phase (26–27 October 2002), we looked at the temporal CSC evolution on the Pernicana Fault plane, in order to see if the stress changes induced by the magmatic intrusions were temporally and spatially correlated with the 27th October earthquake, where the Pernicana Fault was treated as a "passive" (receiving) fault; b) in the second phase (27–29 October 2002), we looked at the CSC on Santa Venerina Fault plane. In this latter case, we evaluated the separate stress changes effect due to the dike-forming intrusions only and, then, to a combination of dike-forming intrusions plus an "active" left-lateral strike slipping Pernicana Fault (western segment), whose movement of several centimeters has been evinced by geological surveys during the eruption period (Neri et al., 2004, 2005). In this case, Pernicana Fault is additionally displaced in order to consider the effect of the pre-stress produced by the action of previous intrusive phenomena (Neri et al., 2004; Bonforte et al., 2007b; Puglisi et al., 2008; Currenti et al., 2012; Alparone et al., 2013a and 2013b; Ruch et al., 2013). We obtained that the dike-forming intrusions are responsible for the activation of Pernicana fault. Moreover, the earthquake on Pernicana fault, combined with the dike-induced stresses, may have triggered the earthquake on Santa Venerina fault.

In the followings, the Mount Etna tectonics and model settings are shown in Sections 2 and 3, results and discussions are presented at Section 4, and finally conclusions are given in Section 5.

2. Tectonic setting and the 2002–2003 eruption

Mount Etna is a basaltic strato-volcano located in the eastern coast of Sicily (Italy) along the front of the collision belt between the African and the Eurasian plates and at the footwall of the Malta Escarpment (a major normal fault system separating the Hyblaean foreland from the thinned Ionian crust, Fig. 1). The volcano is subject to an about N-S striking compressive regime due to the convergence between the two plates (e.g., Cocina et al., 1997; Barberi et al., 2000) and to an extensional, about WNW-ESE, regime, associated to the Malta Escarpment dynamics (e.g., Ellis and King, 1991; Hirn et al., 1997). Together with the two previous described stress regimes, the volcanic edifice is subject to local stress due to magma activities (e.g., Barberi et al., 2000). The analysis

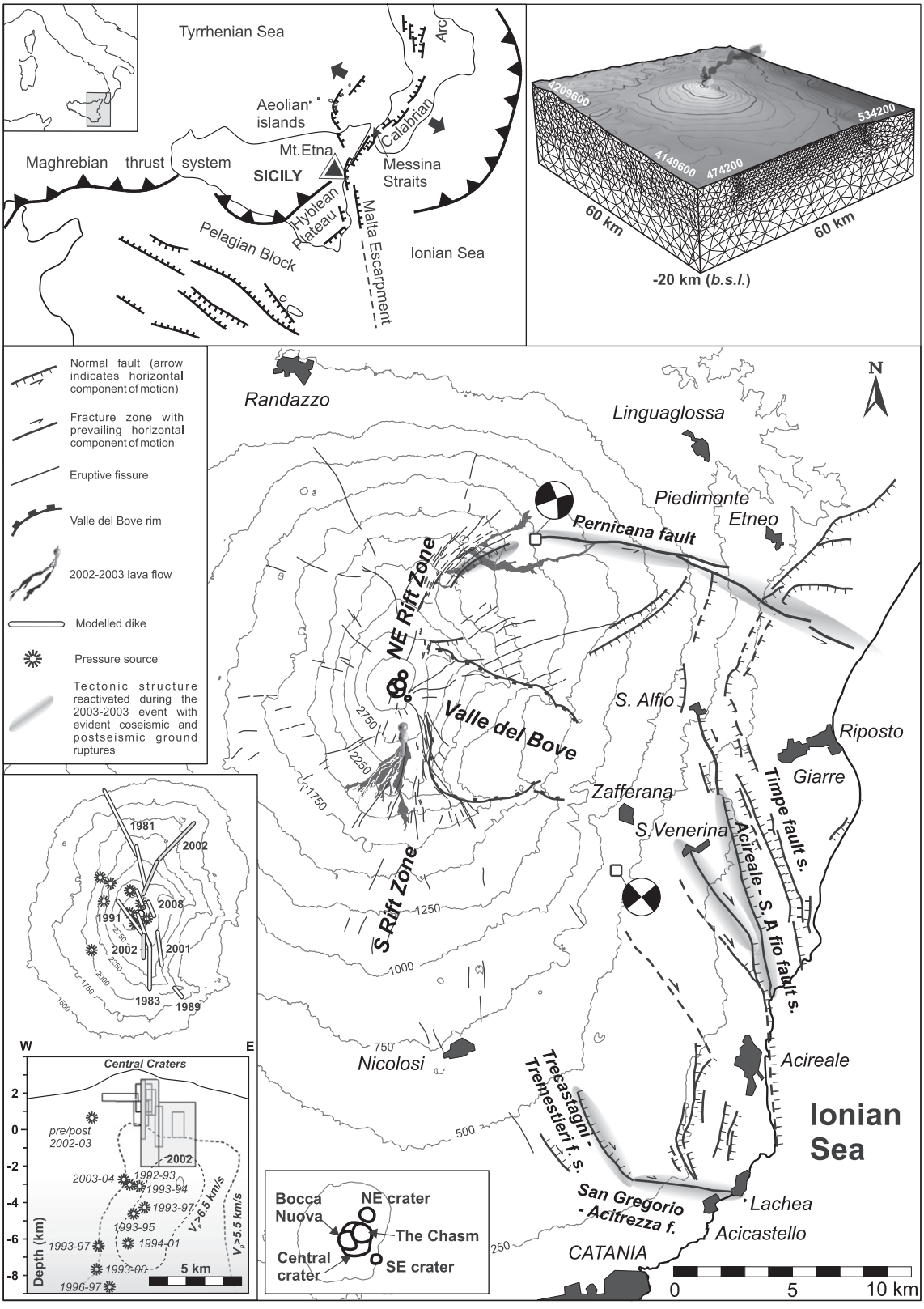

Fig. 1. Map of Mount Etna. A sketch map of the fault systems is reported, together with the most active crustal discontinuities modelled in the paper (heavy black lines) and the NE and south rift zones. The 2002–2003 erupted lava flows and the principal vents are indicated. Moreover, the surface projection of the modelled 2002–2003 dike-forming intrusions is shown (solid gray lines in the lower inset), together with the magma pathways historically resolved by GPS, seismic, and other geophysical data. In the upper inset, the location of Mount Etna in the central Mediterranean area is shown, at the footwall of the Malta Escarpment. Moreover, in the upper inset, the meshed domain is reported. The mesh elements were gradually refined from the domain bottom to the fault systems and the ground surface. Epicentral location and focal mechanisms of the two studied earthquakes are also shown. Redrawn from Aloisi et al. (2011).

of the distribution of the GPS velocity vectors during the inflation and deflation periods suggests that the volcanic edifice can be described as characterized by two kinematically distinct sectors: the western flank that has a scant morphological evidence of faulting or eruptive fracturing and is buttressed to the western and northern part by the Maghrebian Chain, and the eastern flank that is formed by several fault systems accommodating a near constant seaward flank displacement whose origin is still lively debated (for a comprehensive excursus see, e.g., Palano et al., 2008; Palano et al., 2009; Aloisi et al., 2011; Chiocci et al., 2011; Cannavó et al., 2014).

There are principally two types of eruptions at Etna (e.g., Aloisi et al., 2009): a) summit strombolian eruptions, where magma intrudes through the central conduit, and b) dike-forming eruptions that can be lateral (when magma departs horizontally from the central conduit to reach the volcano flank) or eccentric (when magma propagates vertically from several kilometers depth to break out at the surface bypassing the central conduit system). Most of dike-forming intrusions ascend along two rift zones, a) the NE Rift, which is an about 5 km long, 1 km wide, topographic ridge extending between 2500 m and 1850 m (above sea level - hereafter, a.s.l.), made up of lavas and pyroclastics, and b) the S Rift zone, a diffuse set of NNW-SSE to SSW-NNE striking fissures, which extends down to Nicolosi village and is marked by aligned spatter cones coalesced at places to the volcanic ridges (Fig. 1).

Previous studies argued that the 2002 magma intrusion mechanically interacted with pre-existing structures (Northeast Rift and Pernicana Fault), which influenced the stress propagation and were reactivated during dike intrusions (e.g., Acocella et al., 2003; Del Negro et al., 2004; Walter et al., 2005; Currenti et al., 2007; Aloisi et al., 2011). Moreover, the close correlation between seismic activities and magmatic intrusions was provided by previous studies (e.g., Bonforte et al., 2007a; Currenti et al., 2010), which affirmed that the dynamics of Mt. Etna in the summer of 2002 resulted in optimal conditions for the onset of the 2002–2003 eruption, referring, in particular, to the 22 September 2002 ($M_d = 3.7$) earthquake that struck the northeastern part of Mt. Etna and to a consequent tensile mechanism that was detected in the upper part of the Pernicana Fault and was interpreted as a precursor of the eruption that occurred a month later.

The work, here presented, focused on better understanding the described relations between the dike-forming intrusions and the principal fault systems, activated during the 2002–2003 eruption, which is one of the best studied events ever at Mount Etna (e.g., Del Negro et al., 2004; Andronico et al., 2005; Neri et al., 2005; Andronico et al., 2008; Currenti et al., 2008b; Spampinato et al., 2008; Ferlito et al., 2009; De Gori et al., 2011; Steffke et al., 2011), being characterized by diffuse ground fracturing (Neri et al., 2004; Neri et al., 2005), strong explosive activity and petrographically distinct lava outputs and so suitable for the proposed investigation.

The 2002–2003 eruption started late on the night of the 26 October 2002, heralded by only a few hours of premonitory seismicity. After fourteen months of repose succeeding the eruption of July–August 2001, at 20:12 UTC on 26 October 2002, a seismic swarm indicated the beginning of a new eruptive episode. During the first 3–4 h, it took place in the southern-upper part of the volcano (Barberi et al., 2004). A ground-based thermal survey, carried out at 4:00:05 UTC on the 27th, revealed the opening of eruptive fissures on the volcano's southern flank (Spampinato et al., 2008). A first dike-forming intrusion ascended vertically through the volcano edifice (Figs. 1 and 2) in only a few hours and was located south of the summit area (South Rift), close to the 2001 eruption site (Bonaccorso et al., 2002; Aloisi et al., 2003; Aloisi et al., 2006). On 27 October, a second dike-forming intrusion propagated laterally along the NE Rift (Figs. 1 and 2) for a few days (Aloisi et al., 2006). The NE intrusion, active for nine days, demonstrated prevalent strombolian activity, producing a lava volume of about $8–12 \cdot 10^6$ m^3 (Andronico et al., 2005). The southern activity lasted a total of 81 days and was characterized by high explosive and minor effusive activity, that produced a flow field of about $25–34 \cdot 10^6$ m^3. Fire fountaining formed sustained eruptive columns and caused abundant tephra fallout whose volume has been estimated to be $43 \pm 6 \cdot 10^6$ m^3 (Andronico et al., 2008).

The double intrusions were preceded, accompanied and followed by intense seismic activity (874 earthquakes, $M_d \geq 1$, during the whole period), (Barberi et al., 2004; Gambino et al., 2004; Monaco et al., 2005; Neri et al., 2005; De Lorenzo et al., 2010). In particular, most of the seismic energy was released during the first four days (470 events on a total of 874, $M_{max} = 4.4$). Before the onset of the eruption, at 20:25 (GMT) on October 26, 2002 and until 01:28 GMT on 27 October, a seismic swarm took place in the southern and central upper part of Mt. Etna. Successively, the epicentral seismic pattern showed a northeastward migration of earthquakes along the NE Rift (Aloisi et al., 2006). In the early morning of 27 October, seismicity (01.28 GMT, depth = 1.6 km above the sea level (a.s.l.), $M_d = 3.5$; left lateral motion) involved also the western tip of the WNW-ESE trending Pernicana Fault on the northeastern flank of the volcano, destroying the Piano Provenzana skiing station (Gruppo Analisi Dati Sismici, 2014; Alparone et al., 2015). Two days later, on the eastern flank, the Timpe fault system was reactivated with dextral-oblique motion in the area of the Santa Venerina Fault (10.02 GMT, depth = 0.7 km below the sea level (b.s.l.), $M_d = 4.4$; 16.39 GMT, depth = 2.8 km b.s.l., $M_d = 4.0$; 17.14 GMT, depth = 2.2 km b.s.l., $M_d = 4.1$) (Monaco et al., 2005). Moreover, aseismic slip along the San Gregorio-Acitrezza Fault also occurred after the Timpe seismic sequences (Monaco et al., 2011). On 29 October, after a decrease in the earthquake rate, a sharp resumption due to the activation of new seismic structures in south-eastern flank was observed (Monaco et al., 2005). The eruption ended on January 28, 2003.

The deformation pattern recorded during the 2002–2003 eruption was extensively analyzed by analytical (e.g., Aloisi et al., 2003, 2006; Bonforte et al., 2007b) and numerical modelling (e.g., Walter et al., 2005; Currenti et al., 2008a, 2010; Aloisi et al., 2011). The models indicated that the observed displacements can be interpreted as the response of the volcanic edifice to a pair of dike-forming intrusions: a rapid ascent of an eccentric dike-forming intrusion that triggered the eruption in the southern flank and a lateral intrusion of a second dike-like body in the north-eastern flank (Figs. 1 and 2).

3. Model settings

The numerical model presented in this work is an improvement of the analysis performed in Aloisi et al. (2011) and has been developed with the commercial software COMSOL Multiphysics. The model takes into account the topography, the medium heterogeneities, the most active crustal discontinuities, with specified friction coefficients, and the magmatic sources related to the 2002–2003 Etna eruption, described as a set of tabular dislocations (Aloisi et al., 2011), Figs. 1 and 2. We first verified that the dimension of FEM domain was large enough to cancel out any displacements in proximity to the external boundaries, avoiding the generation of artifacts on the solution (Aloisi et al., 2011). Moreover, with the aim of verifying if near field displacements were reproduced with an acceptable accuracy in our numerical domain, we performed a comparison between numerical and analytical displacements produced by the three tabular dislocations, obtaining a standard deviation between the two solutions, on the free surface, of few millimeters (0.003 m). In terms of material characterization, the novelty, with respect to the model developed in Aloisi et al. (2011), is the inclusion of a viscoelastic and of a plastic domain which allow looking at coseismic and postseismic deformations along Pernicana and Santa Venerina faults in a more realistic manner. Viscoelasticity at Mount Etna is motivated by the displacements recorded at Pernicana Fault. In fact, results from post-intrusive GPS monitoring with five months encompassing and following the onset of 2002–03 Mt. Etna eruption showed that, after the end of the northern intrusion, the Pernicana Fault continued to slip and the overall ground deformation pattern may be explained in terms of a time-dependent viscoelastic relaxation

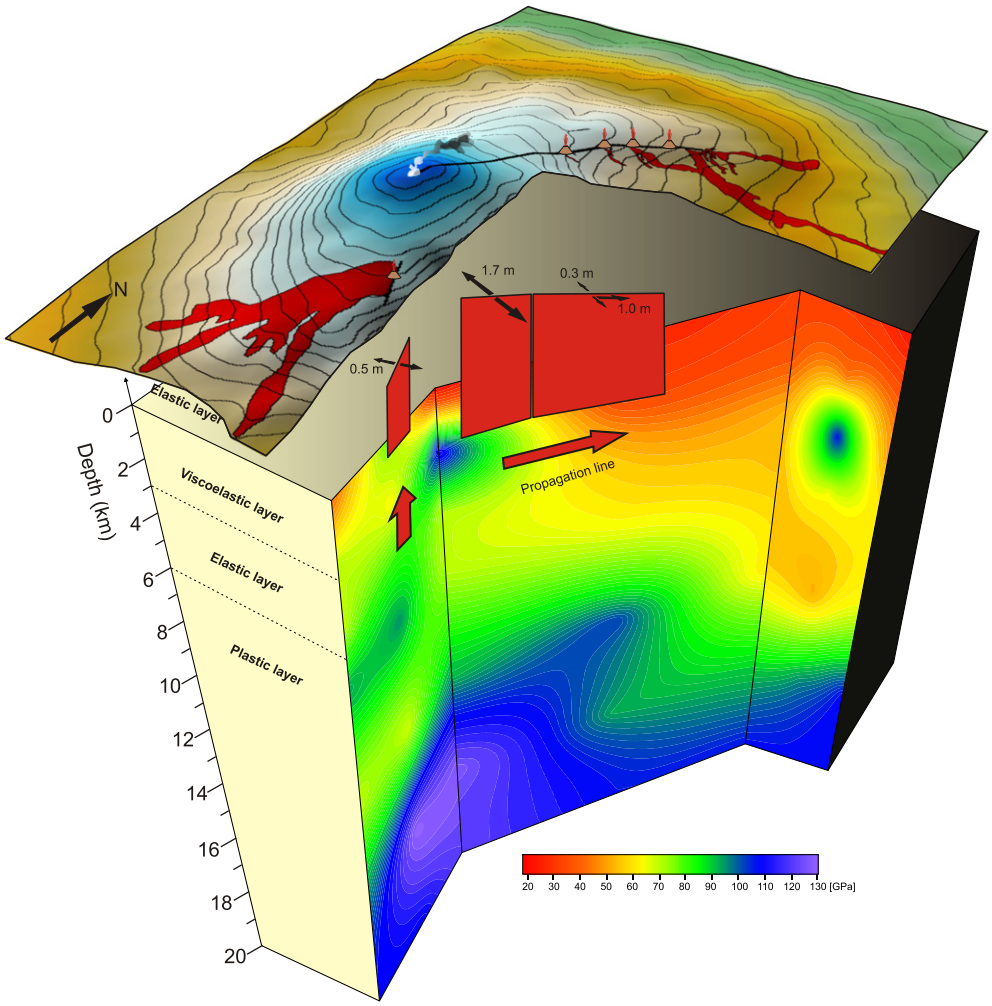

Fig. 2. Time-dependent model with the dimensions of each layer of the introduced rheology. The dike-forming intrusions with the respective dislocation components are showed. Young's modulus deduced by the seismic tomography of Aloisi et al. (2002) is also reported along the cross-section. Redrawn from Aloisi et al. (2006).

process or using an after-slip mechanism (Palano et al., 2009). Either proposed model may explain the observed time-dependent deformation. In volcanic areas, rocks near magmatic sources are considerably heated and viscoelastic relaxation is a mechanism commonly invoked to explain postseismic stress field changes (e.g., Newman et al., 2001; Freed and Lin, 2001; Currenti et al., 2008b). In our work, we evaluated the viscoelastic relaxation approach. In particular, the post-intrusive deformation observed at surface could have been driven by viscoelastic flow, in a weak layer encompassing the clayey sedimentary basement and located below an elastic layer, in response to the stress concentration. We think that this idea is reliable because is compatible with the presence of the about 1 km thick clay layer under the volcanic edifice and of incoherent clay material outcropping along Pernicana Fault together with volcanic rocks, which lowers the viscosity of the lithosphere (usually ~10^{17}–10^{20} Pa*s; Hearn et al., 2002; Hearn, 2003; Sheu and Shieh, 2004). Palano et al. (2009) found values of viscosity for this area ranging between ~7.1×10^{14}–$1.3 \cdot 10^{15}$ Pa*s, lower than those estimated (6.1×10^{16} Pa*s for a relaxation time of 3.5 years) for the relaxation of the basaltic substrate (Briole et al., 1997). It is noteworthy that, Pavlov (1960) obtained viscosity values of about 10^{13} Pa*s for several low melting clays.

Moreover, in active volcanic zones, magmatic activity, heating the surrounding rocks, perturbs the geothermal gradient at relatively shallow crustal level, beyond the brittle-ductile transition temperature. Therefore, heated and weakened rocks at shallow levels, above ~5.0 km (b.s.l.), no longer behave in a purely elastic manner (Del Negro et al., 2009). Worldwide, the interval from ~1.5 km to ~4.0 km (b.s.l.) represents, a region of neutral buoyancy where magma densities and country rock densities are just balanced (e.g., Ryan, 1987, 1993, 1994; Corsaro and Pompilio, 2004). In the last decade, for Etna volcano, many active magmatic sources have been found in correspondence of this zone of neutral buoyancy (e.g., Aloisi et al., 2011; Bruno et al., 2012), along the magma pathways historically resolved by GPS, seismic and other geophysical data (see Aloisi et al. (2011)), bounding a high v_p body (e.g., Aloisi et al., 2002; Patanè et al., 2006). By following these considerations, we considered (Fig. 2) a viscoelastic layer maximum depth of 3 km (b.s.l.), which is compatible with the depth of the neutral buoyancy level (from ~1.5 km to ~4.0 km, b.s.l.) and the depth of the above lying clayey substratum (~1 km thick), including the discontinuously outcroppings along Pernicana Fault and in the eastern flank (Branca and Ferrara, 2001; Bonforte et al., 2007a).

It is noteworthy that, as showed in Singh and Rosenman (1974) and for a vertical strike-slip rectangular fault, the results in using viscoelastic models differ significantly from the corresponding elastic results. According to the above considerations, the application of a viscoelastic rheology could allow us to obtain a model that better approximate the observed behaviour of the volcano. Therefore, we here developed a time-dependent model.

In our model, the viscoelastic behaviour of the medium is represented by using a generalized Maxwell model (e.g., Trasatti et al., 2003; Del Negro et al., 2009), with two spring-dashpot elements. The model is characterized by a shear modulus G_0, as a function of the Young's

modulus and the Poisson's ratio, deduced by the seismic tomography of Aloisi et al. (2002), Fig. 2. Therefore, our domain is inhomogeneous and anisotropic. The fractional shear moduli μ_1 and μ_2 of the two branches, have the same value, equal to 0.5 (Del Negro et al., 2009), however the related relaxation times for each branch are different. This means that even if the viscosity of the dashpots in the two branches is the same, the medium relaxes with different velocities. Starting from the elastic solution proposed by Okada (1992) for a tabular dislocation source embedded in an elastic and homogeneous half-space, Piombo et al. (2007) applied the "Correspondence Principle" of linear viscoelasticity which states that the Laplace transform of the solution to any deformation problem with a linear rheology can be expressed in the form of the corresponding elastic solution, given a suitable choice of Laplace-transformed effective shear modulus. In this way, the authors derived the quasi-static displacement, strain and stress fields for finite rectangular dislocations in a viscoelastic, homogeneous and isotropic half-space, assuming a viscoelastic deformation with respect to both the shear and the normal stresses (keeping a constant bulk modulus) and with a shear modulus relaxing as Maxwell fluid. The relaxation times derived by Piombo et al. (2007) for faults embedded in a viscoelastic halfspace are:

$$\tau_1 \equiv 3\frac{\lambda+\mu}{3\lambda+2\mu}\tau_0 \qquad \tau_2 \equiv 3\frac{\lambda+2\mu}{3\lambda+2\mu}\tau_0 \tag{1}$$

where $\tau_0 = \frac{\eta}{G_0\mu}$ is the Maxwell relaxation time and characterizes the rate of decay of stress, while λ and μ are the first Lamè constant and the shear modulus, respectively and η is the viscosity. The relaxation times are related to the use of two spring-dashpot elements. The use of the relaxation times calculated for a tabular dislocation source (Piombo et al., 2007) is appropriate because it is the same type of dislocation that we used in this work for simulate the dike-forming intrusions (Aloisi et al., 2011), Fig. 2. In our case, however, we are one step further because we consider a heterogeneous 3D domain where the physical properties change both with depth and horizontally based on realistic tomographic results as shown in Aloisi et al. (2002). Therefore, Lamè constants change inside our domain, and, in the same way, the relaxation times. In other terms, each zone relaxes with respect to its "local" relaxation time. This is a great advantage with respect to previous studies, because the relaxation times are not the same for all the studied area but depend on the considered physical properties deduced by the seismic tomography. According to the "Correspondence Principle", the bulk modulus is kept constant while the medium deforms in a viscoelastic manner with respect to both the shear and the normal stresses. In our model, there is no violation of this Principle, since the bulk modulus (as the other constants) is still locally constant. This means that the bulk modulus is constant under the substitution of the new "local" Lamè constants obtained by the Laplace transform, but only for the values that these constants assume in specific zones of the domain.

Below 6 km depth (Fig. 2), we included a plastic layer representing the ductile carbonates substrate corresponding to the Hyblean Plateau that starts at about a depth of 5 km underneath the volcanic edifice and has an average thickness of about 10 km. As said before, Heap et al. (2013) and Bakker et al. (2015) have in fact demonstrated that thermal-stressing induces a progressive and significant change in the physical properties of the Etnean carbonate basement and that, above 500°, the rocks deform in a ductile manner. They speculate that this ductile behaviour could be a key factor in explaining volcano instability. In our model, the plastic behaviour is set in the form of a perfectly plastic material with a yield strength of 300 MPa, which is consistent with experimental values as described in Heap et al. (2013) and Bakker et al. (2015).

No gravitational load is applied because, as demonstrated in Aloisi et al. (2011), its contribution is small with respect to the total displacement and can then be avoided. The other model settings (geometry, mesh and boundary conditions) are referred to Aloisi et al. (2011), Fig. 1.

The aim of our viscoelastic/plastic FEM model is to investigate the temporal link between the push of the 2002–2003 dike-forming intrusions and the movements on the principal fault systems, in relation to the recorded seismicity. In particular, we investigated if the stress change due to the magma intrusion in the S and NE Rift was responsible for the 27 October 2002 Pernicana earthquake (01.28 GMT; $M_d = 3.5$) and for the 29 October 2002 Timpe fault system earthquake (10.02 GMT; $M_d = 4.4$). The path of the magmatic intrusions can be estimated by seismic activity (Barberi et al., 2004; Aloisi et al., 2006). In particular, Barberi et al. (2004) analyzed the spatio-temporal evolution of the epicentral pattern during the period 26–29 October 2002 and Aloisi et al. (2006) analytically modelled the composite intrusion of the two dikes, using seismic and tilt data. These analyses show that, from 21.00 GMT to 23.30 GMT on 26 October, a near vertical tensile dike-forming intrusion propagated on the southern upper flank. Successively, the recorded data show that, from 00.10 GMT on 27 October, a complex dike-forming intrusion propagated laterally along the NE Rift, reaching the western tip of the Pernicana Fault at about 23.00 GMT, 27 October. The intrusion has also been documented by the formation of a series of eruptive fissures and explosive activity in correspondence of the dike path (Spampinato et al., 2008). During the dike-forming intrusions, the first, here studied, earthquake (27 October 2002, 01.28 GMT, $M_d = 3.5$) was recorded. After about thirty-five hours from the starting of the interaction between the NE dike-forming intrusion and the Pernicana Fault, also evidenced by compressive focal mechanism (Barberi et al., 2004; Aloisi et al., 2006), the second, here studied, earthquake (29 October 2002, 10.02 GMT, M_d 4.4) was generated.

Therefore, following the results in time and dislocations obtained from the above, we reproduced the magmatic intrusions by activating the dikes sequentially (Fig. 2). First we activated the south dike (extending from 0.5 km b.s.l. to the volcano surface and having a length of 1.6 km) prescribing an opening component of 0.5 m and, then, the north-east dike, which is modelled in two distinct pieces: a first part (extending from 2.0 km b.s.l. to the volcano surface and having a length of 2.5 km), which has an opening component of 1.7 m and a second part (extending from 2.0 km b.s.l. to the volcano surface and having a length of 3.5 km), which has an opening component of 0.3 m and a left strike slip component of 1 m (Aloisi et al., 2011). All the components of these three dikes are gradually activated in time from zero to each maximum value through a linear function. In particular, the south dike is activated from the beginning of the simulation (21.00 GMT on 26 October) to 2.5 h after (23.30 GMT on 26 October), and then its maximum opening value is kept constant (to avoid a linear backward response). Successively, the first north east dike is gradually activated from 00.10 GMT to 02.00 GMT, on 27 October. Finally, while the south dike and the first north eastern dike opening components are kept at their maximum values, the second part of the north eastern dike is gradually activated from the 02.00 GMT to the 16.00 GMT, on 27 October (Aloisi et al., 2006). All the three magmatic intrusions keep the maximum values of their dislocation components until the end of the simulation, which is set at a total time of 65 h, across the time of occurrence of the M_d 4.4 earthquake, along Santa Venerina Fault (29 October 2002, 10:02 GMT).

To see if Pernicana and Santa Venerina earthquakes were generated by the intrusions, we monitored the variation of the static CSC during the time, considering the intrusions as the sources of the stress change, and looking at the CSC on a left lateral, about E-W, strike-slip fault (western part of Pernicana Fault) and on a right lateral, about NW-SE, strike-slip fault (Timpe fault system). To do this, our time-dependent model is set as following: in the first phase (co-intrusive period), the southern and north-eastern dikes intrude, through the time, as described above and the chosen time step for this phase is half an hour. In the second phase (post-intrusive period), the simulation goes further through the time, until the 29 October, with a time step of 1 h. These

time steps have been chosen after different tests, in order to balance between the computational time and an accurate description of the phenomena.

During the first phase, we verified if the CSC on the Pernicana Fault is big enough to trigger the 01.28 GMT, $M_d = 3.5$, earthquake. In the second phase, we analyzed instead the evolution of the CSC considering two different cases. In the first case, the magma intrusions are considered as the only responsible of the CSC evolution in the area of Santa Venerina Fault. For this case, we computed the CSC values to see if they were big enough to trigger the Santa Venerina earthquake. In the second case instead, we evaluated the combined contribution of the magma intrusions together with the Pernicana earthquake on the Santa Venerina seismicity. In this case, Pernicana fault was activated from the time of the M_d 3.5 earthquake for 30 min, that is the simulation time step, applying a left lateral strike slip component of 0.7 m (Neri et al., 2004), considering the effect of the pre-stress state for acting intrusive dynamics, cumulated during the interseismic period (Neri et al., 2004; Bonforte et al., 2007b; Puglisi et al., 2008; Currenti et al., 2012; Alparone et al., 2013a and 2013b; Ruch et al., 2013). In this way, we kept into account the overall dislocation, along of the Pernicana Fault, produced by the Pernicana earthquake and by the push of the magmatic intrusions. The aim of this investigation is to see if the Santa Venerina earthquake may have been triggered by the Pernicana stress transfer in a chain process, which starts from the South and North-East magma intrusions first. Results of these investigations are showed in the following section.

4. Results and discussions

Fig. 3 shows the temporal evolution of the CSC on Pernicana fault plane at the hypocentral location of the 27th October, 01.28 GMT earthquake (1.6 km, a.s.l.). Three hours after the start of the magma intrusion (00.00 GMT on 27 October), the CSC values are still not enough (0.03 bar) to justify an activation of the fault. As discussed before, the range of stress for triggering an earthquake depends in fact on many factors related to the area of study but it has been shown that, in average, an increment of about 0.1 bar, with respect to the initial stress state, can be enough to trigger an earthquake (Stein, 1999; Bonanno et al., 2011; Privitera et al., 2012; Gonzalez and Palano, 2014). Therefore, at the 00.00 GMT on 27 October, we are surely under this approximate minimum level and consequently, according to our simulations, the southern intrusion was not responsible for the Pernicana earthquake. Three and half hours after the intrusion (00.30 GMT on 27 October, Fig. 3), the CSC reaches a value of about +1.3 bar, surely big enough to trigger Pernicana earthquake that would take place an hour later, when the CSC reaches a value of about +1.5 bar (Fig. 3). Therefore, we found that the first part of the north-east dike intrusion was able to activate Pernicana fault, about when the maximum value of the CSC is reached and consequently our model was able to predict accurately enough the time of the Pernicana earthquake. When the second part of the north-east dike intrudes, the CSC starts to decrease, tending to discourage left-lateral strike slip dislocations. In particular, using the classification of Kaverina et al. (1996) and Kagan (2005), four of the focal mechanisms, recorded few hours after the left-lateral strike slip, M_d 3.5, earthquake, when the CSC becomes negative, show strike-slip together with thrust characteristics (Fig. 3). This behaviour can be interpreted as the effect of the final interaction of the intrusion with the western tip of Pernicana fault, where it slowed and stopped. Also Currenti et al. (2008a) found that the stress change area surrounding Pernicana Fault well matches the seismicity recorded from 27 to 29 October. The boundary elements models, developed by Walter et al. (2005), show a significant increase of the Coulomb failure stress at the western end of the Pernicana Fault. The two models previously mentioned, however, do not consider any dynamic effect as they run stationary. Our model instead is timely dependent and, therefore, for the first time, allowed as to described in detail how the CSC changes evolved in time, increasing and decreasing in response to the emplacement of various dike-forming intrusions. Our model, taking into account the principal fault systems with specified friction coefficients, can explain clearly how etnean faults respond in different manner to the position of magmatic intrusions. Moreover, it allows looking at the CSC directly on the fault plane (Fig. 4). Results show that positive CSC are lower, with respect to the other parts of the fault plane, about at the sea level. Higher CSC values appear in two small areas above and under the sea level. The area included between the free surface and the sea level is in accordance with the estimated hypocentral location (Fig. 4) and is more circumscribed than the results provided by Walter et al. (2005).

Aloisi et al. (2003) found that the north-eastern intrusion was the primary cause of the recorded deformation pattern, while the southern dike gave only a minimal contribution. Our results clearly demonstrated that exactly the NE intrusion is compatible with the reactivation of the

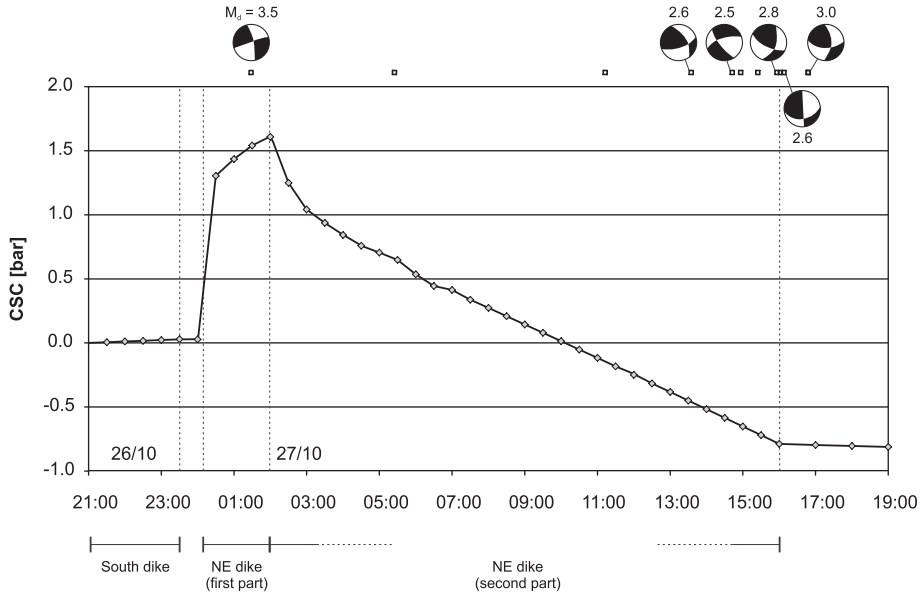

Fig. 3. Temporal evolution of the Coulomb stress changes resolved at the hypocentral location of the 27th October, 01.28 GMT earthquake (1.6 km, a.s.l.). The earthquakes (little squares) recorded in a range of 2 km around the 27th October earthquake, together with the available corresponding focal mechanisms (Barberi et al., 2004), are also reported.

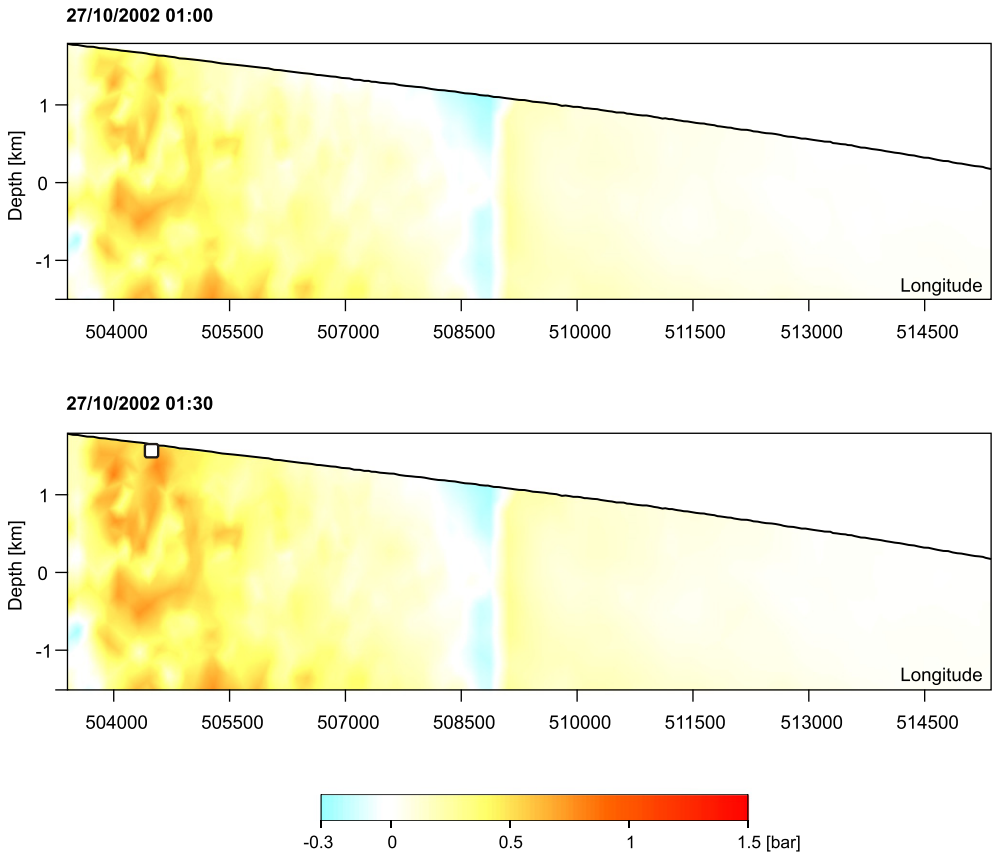

Fig. 4. Coulomb stress changes resolved on Pernicana fault plane at the 01.00 GMT and 01.30 GMT on 27 October, about the time of Pernicana M_d 3.5 earthquake. The white square indicates the hypocentral location of the 27th October, 01.28 GMT earthquake.

Pernicana fault, and, in particular, exclusively the first part of the intrusion. As found by other authors (e.g., Ferlito et al., 2009) this is consistent with the kinematic of the NE Rift, which plays a very active role in the activity of Mt. Etna volcano, for its extensional tectonics, that allows the intrusion and residence of magma bodies at various depths, and for the interaction it has with seismogenetic structures (Neri et

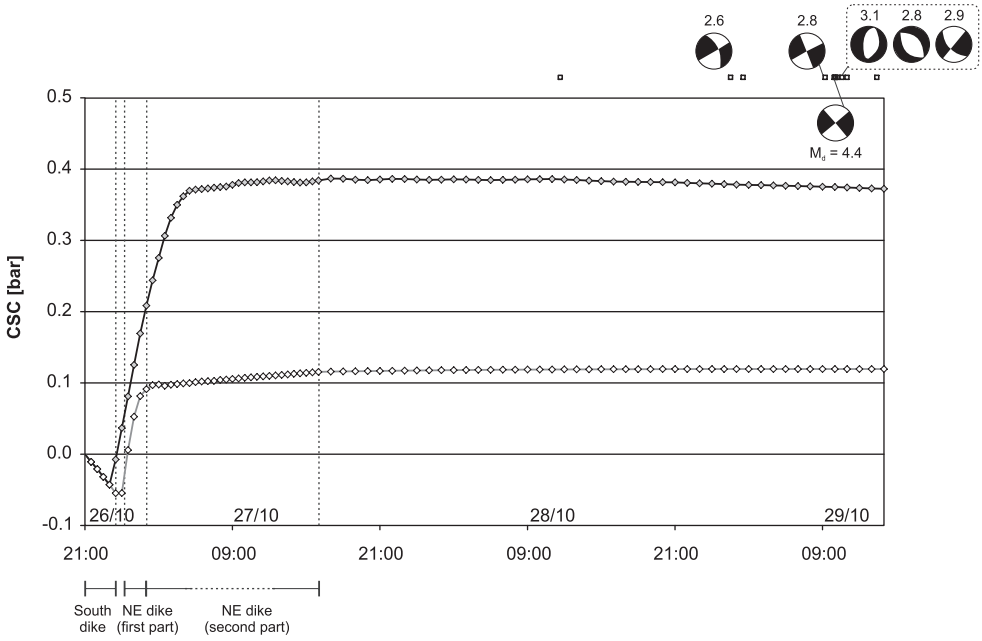

Fig. 5. Temporal evolution of the Coulomb stress changes resolved at the hypocentral location of the 29th October, 10.02 GMT earthquake (0.7 km, b.s.l.). The line with white diamonds reports the CSC as induced by dike-forming intrusions exclusively (Pernicana passive). Whereas, the line with gray diamonds reports the CSC when Pernicana fault is activated. The earthquakes (little squares) recorded in a range of 2 km around the 29th October earthquake, together with the available corresponding focal mechanisms (Barberi et al., 2004; Monaco et al., 2005), are also reported.

al., 2004; Bonforte et al., 2007b; Puglisi et al., 2008; Currenti et al., 2012; Alparone et al., 2013a and 2013b; Ruch et al., 2013).

Fig. 5 shows the temporal evolution of the CSC on the Santa Venerina fault plane at the depth of the 29th October, 10.00 GMT earthquake (0.7 km, b.s.l.). After six hours from the start of the magma intrusions, the CSC for Santa Venerina fault, as induced by dike-forming intrusions exclusively, reached a value of about +0.1 (bar), (line with white diamonds in Fig. 5). This result allows us to infer that, probably, Santa Venerina earthquake could have been triggered by magma intrusions, only. But, as said before, an increment of about 0.1 bar, with respect to the initial stress state, can be seen as an almost lower limit value to trigger an earthquake. Therefore, we decided to verify if there are other active processes that, combined with the dike-induced stresses, can be better explain the Santa Venerina earthquake. Similarly, Currenti et al. (2008a) looked at the static stress changes onto the Timpe fault system and obtained a low value of CSC, compatible with our results. Walter et al. (2005) found instead a negative value, still suggesting that the faulting on the Santa Venerina Fault is discouraged by the dike intrusions. They speculated that this fault was coupled to movement of the Pernicana fault and not so much to shallow level intrusions.

Therefore, might the earthquake on Santa Venerina fault have been triggered by Pernicana fault, in combination with the dike-forming intrusion? This question is plausible if we consider the slip observed on Pernicana Fault, unlocked by the 2002–2003 magmatic intrusion, as the result of the stress accumulated during inter-seismic periods by response to previous intrusive dynamics, acting on the high eastern and northeastern portion of the volcano. According to this point of view, the slip observed on Pernicana Fault would have two components, (a) the push of the dike-intrusions and (b) the movement related to the stress previously accumulated and then suddenly released, during the M_d 3.5 earthquake. Consequently, Pernicana Fault (that, until now, has been treated as a passive receiving crustal discontinuity) has to be activated, exclusively in the western segment, by choosing the value of slip that this segment had during the first day of eruption, according to field campaign measurements (about 0.7 m of strike slip component; Neri et al., 2004). When Pernicana Fault is activated, the CSC value on Santa Venerina Fault rises up to about +0.4 bar in circa 20 h, (line with gray diamonds in Fig. 5), which is higher with respect to the 0.1 bar, value acceptable for encouraging the fault movement. Also Walter et al. (2005) proposed that Pernicana left-lateral faulting encouraged the movement along Santa Venerina Fault, pointing out to the importance of the fault-fault interaction (see also Neri et al., 2004). However, differently from Walter et al. (2005) that imposed a left-lateral displacement along the entire Pernicana Fault, we obtained that the faulting of the western segment only could have been already enough to encourage the start of the seismic swarms at the Timpe fault system. In fact, if we observe the CSC

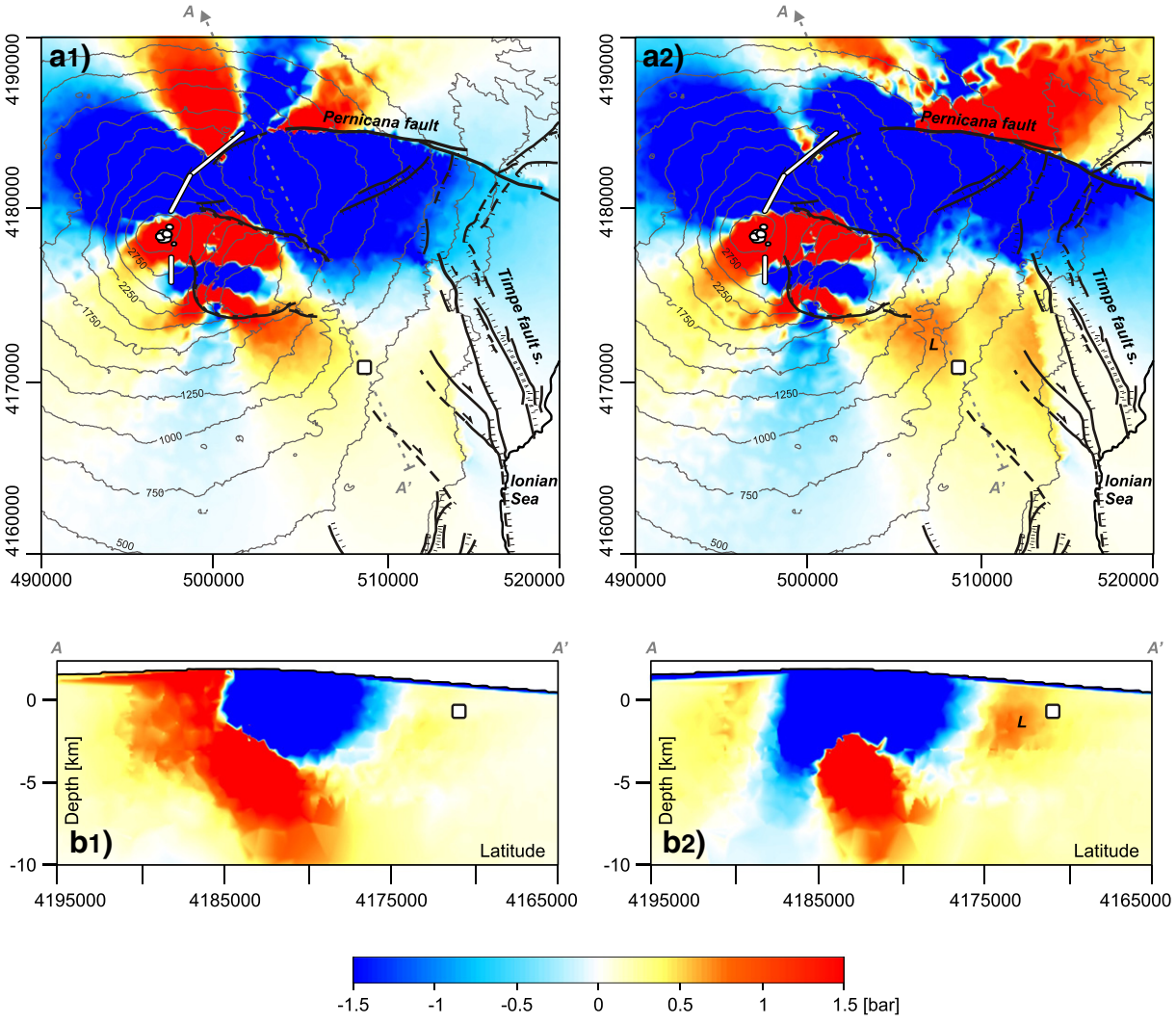

Fig. 6. Coulomb stress changes resolved, at the time of Santa Venerina earthquake (10.02 GMT on the 29th October), along a mapview at 0.7 km b.s.l. (hypocentral depth), in the case Pernicana passive (a1) and active (a2) and along a cross-section passing through the profile AA′, in the case Pernicana passive (b1) and active (b2). The white square indicates the location of the 29th October earthquake. The letter "L" indicates the positive lobe extending much further southwards and eastwards when Pernicana fault is activated (see text for details).

(Fig. 6), at the time of the Santa Venerina earthquake, on an horizontal plane cutting the domain at the hypocentral depth (0.7 km b.s.l.), the positive lobe "L" in the area of the earthquake is much more wide when Pernicana fault is activated (Fig. 6a2) with respect to the case when only the effects of the magmatic intrusions are considered (Fig. 6a1). In particular, the lobe "L" extends much further southwards and eastwards, reaching the Timpe fault systems (Fig. 6a2). The comparison between the two cases above is also clear at depth (Fig. 6b1 and Fig. 6b2). Cutting the domain vertically along an about NW-SE slice (profile AA′) passing through the Santa Venerina fault, we obtained a clearly positive CSC zone, corresponding with the hypocentral depth when Pernicana fault is activated ("L" in Fig. 6b2).

Alparone et al. (2013b) revealed a significant temporal correlation between periods of large deformation of the eastern flank and intensified seismic activity along the northern border (Pernicana fault system). For example, the seismicity along Pernicana fault system, recorded in the 1984, was followed by an increased deformation rate of the eastern flank that continued until 1987. Between 1987 and 2001, the seismicity and the deformations were both reduced. Azzaro et al. (2013) confirmed that the local seismicity is closely related to the flank dynamics and, in particular, they underlined the important role of the Timpe fault system in the seismic hazard affecting the eastern flank. Therefore, the common temporal evolution of the Pernicana kinematics and of the eastern flank activity demonstrates that there is a clear correlation between the two processes, as we also obtained.

Regarding the temporal evolution of the CSC on Santa Venerina fault (Fig. 5), our model is not able to predict exactly the time of the M_d 4.4 earthquake because the maximum CSC value is reached several hours before, about at the end of the north-east intrusion time and this value remains more or less constant during the time. However, during this time interval, some earthquakes were recorded in the area around the M_d 4.4 earthquake, showing a kinematic compatible with the estimated CSC (Fig. 5). Moreover, across the end of our simulation, other two strong earthquakes were recorded in the South East sector (29 October 16.39 GMT, $M_d = 4.0$ and 17.14 GMT, $M_d = 4.1$) showing focal mechanisms compatible with the Santa Venerina M_d 4.4 earthquake (Monaco et al., 2005) and, therefore, well explained by our model.

Finally, is noteworthy to say that the presence of the ductile substrate (carbonates) does not appear to be affected, in term of stress, by the dike intrusions. In particular, the maximum stress induced in the ductile layer by the intruding dikes is about 1 MPa, which is one order of magnitude lower than the minimum yield stress (10 MPa) for such rocks at this depth and under thermal weakening condition (Heap et al., 2013; Bakker et al., 2015).

5. Conclusions

A 3D highly realistic FEM numerical model has been carried out to investigate the temporal evolution of CSC caused by dyke-forming intrusions during the 2002–2003, Mt. Etna eruption, in a viscoelastic/plastic rheology. The model allowed us to describe in detail how the CSC evolved in time, increasing and decreasing in response to the emplacement of various dike-forming intrusions. Therefore, our model can explain better how etnean faults respond in different manner to the position of magmatic intrusions. It has been showed that the dike-forming intrusions are responsible for the activation of Pernicana fault accordingly to the time and position of the 27th October 2002, 01:28 GMT earthquake ($M_d = 3.5$). Moreover, the earthquake on Pernicana fault, combined with the dike-induced stresses, may have triggered the earthquake on Santa Venerina fault (29 October 10:02 GMT, $M_d = 4.4$). Our results confirm the significant interplay between the processes observed in the eastern flank and underline the key role of the NE Rift in the activity of Mt. Etna volcano. Therefore, the knowledge of stress change rates is a powerful tool for assessing seismic hazards, as it cannot only be used to understand past events, but also to predict where future earthquakes are likely to occur.

Acknowledgments

This work was supported by MED-SUV FP7 Project (Grant number 308665). We thank Danila Scandura for the debate about governing equations for ground deformation. We thank Antonio Scaltrito and Graziella Barberi (INGV, Osservatorio Etneo, Catania) for the fruitful discussion on the 2002–2003 etnean seismicity. We thank Luciano Scarfì for the discussion about the estimated focal mechanisms. We thank Salvo Gambino for the tips about the explanation of the results. Finally, we thank Mimmo Palano and Flavio Cannavò for the general tips.

References

Acocella, V., Behncke, B., Neri, M., DAmico, S., 2003. Link between major flank slip and 2002–2003 eruption at Mt. Etna (Italy). Geophys. Res. Lett. 30 (24):2286. http://dx.doi.org/10.1029/2003GL018642.

Aloisi, M., Cocina, O., Neri, G., Orecchio, B., Privitera, E., 2002. Seismic tomography of the crust underneath the Etna volcano, Sicily. Phys. Earth Planet. Inter. 134:139–155. http://dx.doi.org/10.1016/S0031-9201(02) 00153-X.

Aloisi, M., Bonaccorso, A., Gambino, S., Mattia, M., Puglisi, G., 2003. Etna 2002 eruption imaged from continuous tilt and GPS data. Geophys. Res. Lett. 30 (23):2214. http://dx.doi.org/10.1029/2003GL018896.

Aloisi, M., Bonaccorso, A., Gambino, S., 2006. Imaging composite dike propagation (Etna, 2002 case). J. Geophys. Res. 111, B06404. http://dx.doi.org/10.1029/2005JB003908.

Aloisi, M., Bonaccorso, A., Cannavò, F., Gambino, S., Mattia, M., Puglisi, G., Boschi, E., 2009. A new dike intrusion style for the Mount Etna May 2008 eruption modelled through continuous tilt and GPS data. Terra Nova 21:316–321. http://dx.doi.org/10.1111/j.1365-3121.2009.00889.x.

Aloisi, M., Mattia, M., Monaco, C., Pulvirenti, F., 2011. Magma, faults, and gravitational loading at Mount Etna: the 2002–2003 eruptive period. J. Geophys. Res. 116, B05203. http://dx.doi.org/10.1029/2010JB007909.

Alparone, S., Cocina, O., Gambino, S., Mostaccio, A., Spampinato, S., Tuvè, T., Ursino, A., 2013a. Seismological features of the Pernicana–Provenzana fault system (Mt. Etna, Italy) and implications for the dynamics of northeastern flank of the volcano. J. Volcanol. Geotherm. Res. 251:16–26. http://dx.doi.org/10.1016/j.jvolgeores.2012.03.010.

Alparone, S., Bonaccorso, A., Bonforte, A., Currenti, G., 2013b. Long-term stress-strain analysis of volcano flank instability: the eastern sector of Etna from 1980 to 2012, J. Geophys. Res. Solid Earth 118:5098–5108. http://dx.doi.org/10.1002/jgrb.50364.

Alparone, S., Maiolino, V., Mostaccio, A., Scaltrito, A., Ursino, A., Barberi, G., D'Amico, S., Di Grazi, a.G., Giampiccolo, E., Musumeci, C., Scarfì, L., Zuccarello, L., 2015. Instrumental seismic catalogue of Mt. Etna earthquakes (Sicily, Italy): ten years (2000−2010) of instrumental recordings. Ann. Geophys. 58 (4), S0435. http://dx.doi.org/10.4401/ag-6591.

Anderson, G., Johnson, H., 1999. A new statistical test for static stress triggering: application to the 1987 Superstition Hills earthquake sequence. J. Geophys. Res. 104: 20153–20168. http://dx.doi.org/10.1029/1999JB900200.

Andronico, D., Branca, S., Calvari, S., Burton, M., Caltabiano, T., Corsaro, R.A., Del Carlo, P., Garfì, G., Lodato, L., Miraglia, L., Murè, F., Neri, M., Pecora, E., Pompilio, M., Salerno, S., Spampinato, L., 2005. A multi-disciplinary study of the 2002-03 Etna eruption: insights into a complex plumbing system. Bull. Volcanol. 67:314–330. http://dx.doi.org/10.1007/s00445-004-0372-8.

Andronico, D., Scollo, S., Caruso, S., Cristaldi, A., 2008. The 2002–03 Etna explosive activity: tephra dispersal and features of the deposits. J. Geophys. Res. 113, B04209. http://dx.doi.org/10.1029/2007JB005126.

Azzaro, R., D'Amico, S., Peruzza, L., Tuvè, T., 2013. Probabilistic seismic hazard at Mt. Etna (Italy): the contribution of local fault activity in mid-term assessment. J. Volcanol. Geotherm. Res. 251:158–169. http://dx.doi.org/10.1016/j.jvolgeores.2012.06.005.

Bakker, R.R., Violaya, M.E.S., Benson, P.M., Vinciguerra, S.C., 2015. Ductile flow in sub-volcanic carbonate basement as the main control for edifice stability: new experimental insights. Earth Planet. Sci. Lett. 430:533–541. http://dx.doi.org/10.1016/j.epsl.2015.08.017.

Barberi, G., Cocina, O., Neri, G., Privitera, E., Spampinato, S., 2000. Volcanological inferences from seismic strain tensor computations at Mt. Etna volcano, Sicily. Bull. Volcanol. 62, 318–330.

Barberi, G., Cocina, O., Maiolino, V., Musumeci, C., Privitera, E., 2004. Insight into Mt. Etna (Italy) kinematics during the 2002–2003 eruption as inferred from seismic stress and strain tensors. Geophys. Res. Lett. 31, L21614. http://dx.doi.org/10.1029/2004GL020918.

Bonaccorso, A., Aloisi, M., Mattia, M., 2002. Dike emplacement forerunning the Etna July 2001 eruption modeled through continuous tilt and GPS data. Geophys. Res. Lett. 29 (13):1624. http://dx.doi.org/10.1029/2001GL014397.

Bonanno, A., Palano, M., Privitera, E., Gresta, S., Puglisi, G., 2011. 2011. Magma intrusion mechanisms and redistribution of seismogenic stress at Mt. Etna volcano (1997-1998). Terra Nova 23:339–348. http://dx.doi.org/10.1111/j.1365-3121.2011.01019.x.

Bonforte, A., Gambino, S., Guglielmino, F., Obrizzo, F., Palano, M., Puglisi, G., 2007a. Ground deformation modeling of flank dynamics prior to the 2002 eruption of Mt. Etna. Bull. Volcanol. 69:757–768. http://dx.doi.org/10.1007/s00445-006-0106-1.

Bonforte, A., Carbone, D., Greco, F., Palano, M., 2007b. Intrusive mechanism of the 2002 NE-rift eruption at Mt Etna (Italy) modelled using GPS and gravity data. Geophys. J. Int. 169:339–347. http://dx.doi.org/10.1111/j.1365-246X.2006.03249.x.

Branca, S., Ferrara, V., 2001. An example of river pattern evolution produced during the lateral growth of a central polygenic volcano: the case of the Alcantara river system, Mt Etna (Italy). Catena 45 (2):85–102. http://dx.doi.org/10.1016/S0341-8162(01)00144-8.

Briole, P., Massonnet, D., Delacourt, C., 1997. Post-eruptive deformation associated with the 1986–87 and 1989 lava flows of Etna detected by radar interferometry. Geophys. Res. Lett. 24:37–40. http://dx.doi.org/10.1029/96GL03705.

Bruno, V., Mattia, M., Aloisi, M., Palano, M., Cannavò, F., Holt, W.E., 2012. Ground deformations and volcanic processes as imaged by CGPS data at Mt. Etna (Italy) between 2003 and 2008. J. Geophys. Res. Solid Earth 117, B07208. http://dx.doi.org/10.1029/2011JB009114.

Cai, J.G., 2001. Effects of parallel fractures on wave attenuation in rock. School of Civil and Structural Engineering, PhD Thesis. Nanyang Technological University, Singapore, p. 306.

Calais, E., Freed, A., Mattioli, G., Amelung, F., J'onsson, S., Jansma, P., Hong, S.H., Dixon, T., Prepetit, C., Momplaisir, R., 2010. The January 12, 2010, Mw 7.0 earthquake in Haiti: context and mechanism from an integrated geodetic study. Nat. Geosci. http://dx.doi.org/10.1038/NGEO992.

Cannavó, F., Arena, A., Monaco, C., 2014. Local geodetic and seismic energy balance for shallow earthquake prediction. J. Seismol.:1–8 http://dx.doi.org/10.1007/s10950-014-9446-z.

Chiarabba, C., Amato, A., Boschi, E., Barberi, E., 2000. Recent seismicity and tomographic modeling of the Mount Etna plumbing system. J. Geophys. Res. 105:10923–10938. http://dx.doi.org/10.1029/1999JB900427.

Chiocci, F.L., Coltelli, M., Bosman, A., Cavallaro, D., 2011. Continental margin large-scale instability controlling the flank sliding of Etna volcano. Earth Planet. Sci. Lett. 305 (1–2):57–64. http://dx.doi.org/10.1016/j.epsl.2011.02.040 (1 May 2011).

Cocina, O., Neri, G., Privitera, E., Spampinato, S., 1997. Stress tensor computations in the Mount Etna area (southern Italy) and tectonic implications. J. Geodyn. 23:109–127. http://dx.doi.org/10.1016/S0264-3707(96)00027-0.

Corsaro, R.A., Pompilio, M., 2004. Buoyancy-controlled eruption of magmas at Mt Etna. Terra Nova 16:16–22. http://dx.doi.org/10.1046/j.1365-3121.2003.00520.x.

Currenti, G., Del Negro, C., Johnston, V., Sasai, Y., 2007. Close temporal correspondence between geomagnetic anomalies and earthquakes during the 2002–2003 eruption of Etna volcano. J. Geophys. Res. 112, B09103. http://dx.doi.org/10.1029/2007JB005029.

Currenti, G., Del Negro, C., Ganci, G., Williams, C.A., 2008a. Static stress changes induced by the magmatic intrusions during the 2002-2003 Etna eruption. J. Geophys. Res. 113, B10206. http://dx.doi.org/10.1029/2007JB005301.

Currenti, G., Piombo, A., Del Negro, C., Dragoni, M., 2008b. Piezomagnetic fields due to an inclined rectangular fault in a viscoelastic half-space: an application to the 2002–2003 Etna eruption. Geophys. J. Int. 175 (3):901–912. http://dx.doi.org/10.1111/j.1365-246X.2008.03941.x.

Currenti, G., Bonaccorso, A., Del Negro, C., Guglielmino, F., Scandura, D., Boschi, E., 2010. FEM-based inversion for heterogeneous fault mechanisms: application at Etna volcano by DInSAR data. Geophys. J. Int. 183 (2):765–773. http://dx.doi.org/10.1111/j.1365-246X.2010.04769.x.

Currenti, G., Solaro, G., Napoli, R., Pepe, A., Bonaccorso, A., Del Negro, C., Sansosti, E., 2012. Modeling of ALOS and COSMO-SkyMed satellite data at Mt Etna: implications on relation between seismic activation of the Pernicana fault system and volcanic unrest. Remote Sens. Environ. 125:64–72. http://dx.doi.org/10.1016/j.rse.2012.07.008.

De Gori, P., Chiarabba, C., Giampiccolo, E., Martinez-Arèvalo, C., Patanè, D., 2011. Body wave attenuation heralds incoming eruptions at Mount Etna. Geology 39:503–506. http://dx.doi.org/10.1130/G31993.1.

Del Negro, C., Currenti, G., Napoli, R., Vicari, A., 2004. Volcanomagnetic changes accompanying the onset of the 2002–2003 eruption of Mt. Etna (Italy). Earth Planet. Sci. Lett. 229:1–14. http://dx.doi.org/10.1016/j.epsl.2004.10.033.

Del Negro, C., Currenti, G., Scandura, D., 2009. Temperature-dependent viscoelastic modeling of ground deformation: application to Etna volcano during the 1993–1997 inflation period. Phys. Earth Planet. Inter. 172 (3–4):299–309. http://dx.doi.org/10.1016/j.pepi.2008.10.019.

De Lorenzo, S., Giampiccolo, E., Martinez-Arevalo, C., Patanè, D., Romeo, A., 2010. Fault plane orientations of microearthquakes at Mt. Etna from the inversion of P-wave rise times. J. Volcanol. Geotherm. Res. 189:247–256. http://dx.doi.org/10.1016/j.jvolgeores.2009.11.011.

Dragoni, M., Bonafede, M., Boschi, E., 1982. Stress relaxation in the earth and seismic activity. Rivista del Nuovo Cimento 5 (2):1–34. http://dx.doi.org/10.1007/BF02740828.

Ellis, M., King, G., 1991. Structural control of flank volcanism in continental rifts. Science 254:839–842. http://dx.doi.org/10.1126/science.254.5033.839.

Ferlito, C., Coltorti, M., Cristofolini, P., Giacomoni, P.P., 2009. The contemporaneous emission of low-K and high-K trachybasalts and the role of the NE Rift during the 2002 eruptive event, Mt. Etna, Italy. Bull. Volcanol. 71 (5):575–587. http://dx.doi.org/10.1007/s00445-008-0243-9.

Feuillet, N., Cocco, M., Musumeci, C., Nostro, C., 2006. Stress interaction between seismic and volcanic activity at Mt. Etna. Geophys. J. Int. 164:697–718. http://dx.doi.org/10.1111/j.1365-246X.2005.02824.x.

Freed, A.M., Lin, J., 1998. Time-dependent changes in failure stress following thrust earthquakes. J. Geophys. Res. 103. http://dx.doi.org/10.1029/98JB01764 (24393 ± 24410).

Freed, A.M., Lin, J., 2001. Delayed triggering of the 1999 Hector Mine earthquake by viscoelastic stress transfer. Nature 411:180–183. http://dx.doi.org/10.1038/35075548.

Gambino, S., Mostaccio, A., Patanè, D., Scarfì, L., Ursino, A., 2004. High-precision locations of the microseismicity preceding the 2002–2003 Mt. Etna eruption. Geophys. Res. Lett. 31, L18604. http://dx.doi.org/10.1029/2004GL020499.

Gonzalez, P.J., Palano, M., 2014. Mt. Etna 2001 eruption: new insights into the magmatic feeding system and the mechanical response of the western flank from a detailed geodetic dataset. J. Volcanol. Geotherm. Res. 274:108–121. http://dx.doi.org/10.1016/j.jvolgeores.2014.02.001.

Gross, S., Kisslinger, C., 1997. Estimating tectonic stress rate and state with Landers aftershocks. J. Geophys. Res. 102:7603–7612. http://dx.doi.org/10.1029/96JB03741.

Gruppo Analisi Dati Sismici, 2014. Catalogo dei terremoti della Sicilia Orientale - Calabria Meridionale (1999–2014). INGV, Catania. http://www.ct.ingv.it/ufs/analisti/catalogolist.php.

Harris, R.A., Simpson, R.W., 1992. Changes in static stress on southern California faults after the 1992 Landers earthquake. Nature 360:251–254. http://dx.doi.org/10.1038/360251a0.

Harris, R.A., 1998. Introduction to special section: stress triggers, stress shadows, and implications for seismic hazard. J. Geophys. Res. 103 (B10):24,347–24,358. http://dx.doi.org/10.1029/98JB01576.

Heap, M.J., Mollo, S., Vinciguerra, S., Lavallée, Y., Hess, K.U., Dingwell, D.B., Baud, P., Iezzi, G., 2013. Thermal weakening of the carbonate basement under Mt. Etna volcano (Italy): implications for volcano instability. J. Volcanol. Geotherm. Res. 250:42–60. http://dx.doi.org/10.1016/j.jvolgeores.2012.10.004.

Hearn, E.H., Bürgmann, R., Reilinger, R., 2002. Dynamics of Izmit earthquake postseismic deformation and loading of the Düzce earthquake hypocenter. Bull. Seismol. Soc. Am. 92:172–193. http://dx.doi.org/10.1785/0120000832.

Hearn, E.H., 2003. What can GPS data tell us about the dynamics of post-seismic deformation? Geophys. J. Int. 155:753–777. http://dx.doi.org/10.1111/j.1365-246X.2003.02030.x.

Hill, D.P., Pollitz, F., Newhall, C., 2002. Earthquake-volcano interactions. Phys. Today 55:41–47. http://dx.doi.org/10.1063/1.1535006.

Hirn, A., Nicolich, R., Gallart, J., Laigle, M., Cernobori, L., ETNASEIS Scientific Group, 1997. Roots of Etna volcano in faults of great earthquakes. Earth Planet. Sci. Lett. 148:171–191. http://dx.doi.org/10.1016/S0012-821X(97)00023-X.

Hyodo, M., Hirahara, K., 2004. GeoFEM kinematic earthquake cycle simulation in Southwest Japan. Pure Appl. Geophys. 164:2069–2090. http://dx.doi.org/10.1007/s00024-004-2549-7.

Jaumé, S.C., Sykes, L.R., 1992. Change in the state of stress on the southern San Andreas fault resulting from the California earthquake sequence of April to June 1992. Science 258:1325–1328. http://dx.doi.org/10.1126/science.258.5086.1325.

Kagan, Y.Y., 2005. Double-couple earthquake focal mechanism: random rotation and display. Geophys. J. Int. 163 (3):1065–1072. http://dx.doi.org/10.1111/j.1365-246X.2005.02781.x.

Kamatchi, P., Ramana, G.V., Nagpal, A.K., Iyer, N.R., 2013. Modelling propagation of stress waves through soil medium for ground response analysis. Engineering 5:611–621. http://dx.doi.org/10.4236/eng.2013.57073.

Kaverina, A.N., Lander, A.V., Prozorov, A.G., 1996. Global creepex distribution and its relation to earthquake-source geometry and tectonic origin. Geophys. J. Int. 125:249–265. http://dx.doi.org/10.1111/j.1365-246X.1996.tb06549.x.

Kenner, S., Segall, P., 1999. Time-dependence of the stress shadowing effect and its relation to the structure of the lower crust. Geology 27:119–122. http://dx.doi.org/10.1130/0091-7613.

Kilb, D., Gomber, J., Bodin, P., 2000. Triggering of earthquake aftershocks by dynamic stresses. Nature 408:570–574. http://dx.doi.org/10.1038/35046046.

King, G.C.P., Stein, R.S., Lin, J., 1994. Static stress changes and the triggering of earthquakes. Bull. Seismol. Soc. Am. 84, 935–953.

Marzocchi, W., Casarotti, E., Piersanti, A., 2002. Modeling the stress variations induced by great earthquakes on the largest volcanic eruptions of the 20th century. J. Geophys. Res. 107. http://dx.doi.org/10.1029/2001JB001391.

Mattia, M., Patanè, D., Aloisi, M., Amore, M., 2007. Faulting on the western flank of Mt Etna and magma intrusions in the shallow crust. Terra Nova 19:1–6. http://dx.doi.org/10.1111/j.1365-3121.2006.00724.x.

Monaco, C., Catalano, S., Cocina, O., De Guidi, G., Ferlito, C., Gresta, S., Musumeci, C., Tortorici, L., 2005. Tectonic control on the eruptive dynamics at Mt. Etna volcano (eastern Sicily) during the 2001 and 2002–2003 eruptions. J. Volcanol. Geotherm. Res. 144:221–233. http://dx.doi.org/10.1016/j.jvolgeores.2004.11.024.

Monaco, C., De Guidi, G., Ferlito, C., 2011. The morphotectonic map of Mt. Etna. It. J. Geosci. 129:409–428. http://dx.doi.org/10.3301/IJG.2010.11.

Neri, M., Acocella, V., Behncke, B., 2004. The role of the Pernicana fault system in the spreading of Mt. Etna (Italy) during the 2002–2003 eruption. Bull. Volcanol. 66:417–430. http://dx.doi.org/10.1007/s00445-003-0322-x.

Neri, M., Acocella, V., Behncke, B., Maiolino, V., Ursino, A., Velardita, R., 2005. Contrasting triggering mechanisms of the 2001 and 2002–2003 eruptions of Mount Etna (Italy). J. Volcanol. Geotherm. Res. 144:235–255. http://dx.doi.org/10.1016/j.jvolgeores.2004.11.025.

Newman, A.V., Dixon, T.H., Ofoegbu, G.I., Dixon, J.E., 2001. Geodetic and seismic constraints on recent activity at Long Valley Caldera, California: evidence for viscoelastic rheology. J. Volcanol. Geotherm. Res. 105:183–206. http://dx.doi.org/10.1016/S0377-0273(00)00255-9.

Nostro, C., Stein, R.S., Cocco, M., Belardinelli, M.E., Marzocchi, W., 1998. Two-way coupling between Vesuvius eruptions and southern Apennine earthquakes (Italy) by elastic stress transfer. J. Geophys. Res. 103 (B10):24,487–24,504. http://dx.doi.org/10.1029/98JB00902.

Okada, Y., 1992. Internal deformation due to shear and tensile faults in a half-space. Bull. Seismol. Soc. Am. 82 (2), 1018–1040.

Palano, M., Puglisi, G., Gresta, S., 2008. Ground deformation patterns at Mt. Etna from 1993 to 2000 from joint use of InSAR and GPS techniques. J. Volcanol. Geotherm. Res. 169:99–120. http://dx.doi.org/10.1016/j.jvolgeores.2007.08.014.

Palano, M., Gresta, S., Puglisi, G., 2009. Time-dependent deformation of the eastern flank of Mt. Etna: After-slip or viscoelastic relaxation. Tectonophysics 473 (3–4):300–311. http://dx.doi.org/10.1016/j.tecto.2009.02.047.

Patanè, D., Mattia, M., Aloisi, M., 2005. Shallow intrusive processes during 2002-2004 and current volcanic activity on Mt. Etna. Geophys. Res. Lett. 32, L06302. http://dx.doi.org/10.1029/2004GL021773.

Patanè, D., Barberi, G., Cocina, O., De Gori, P., Chiarabba, C., 2006. Time-resolved seismic tomography detects magma intrusions at Mount Etna. Science 313:821. http://dx.doi.org/10.1126/science.1127724.

Pavlov, V.F., 1960. The use of the torsional method for determining the viscosity of low melting clays. Glas. Ceram. 16:278–283. http://dx.doi.org/10.1007/BF00695633.

Piombo, A., Tallarico, A., Dragoni, M., 2007. Displacement, strain and stress fields due to shear and tensile dislocations in a viscoelastic half-space. Geophys. J. Int. 170: 1399–1417. http://dx.doi.org/10.1111/j.1365-246X.2007.03283.x.

Pollitz, F.F., Sacks, I.S., 1997. The 1995 Kobe, Japan, earthquake: a long-delayed aftershock of the offshore 1944 Tonankai and 1946 Nankaido earthquakes. Bull. Seismol. Soc. Am. 87, 1–10.

Privitera, E., Bonanno, A., Gresta, S., Nunnari, G., Puglisi, G., 2012. Triggering mechanisms of static stress on Mount Etna volcano. An application of the boundary element method. J. Volcanol. Geotherm. Res. 245–246 (2012):149–158. http://dx.doi.org/10.1016/j.jvolgeores.2012.08.012.

Puglisi, G., Bonforte, A., Ferretti, A., Guglielmino, F., Palano, M., Prati, C., 2008. Dynamics of Mount Etna before, during, and after the July–August 2001 eruption inferred from GPS and differential synthetic aperture radar interferometry data. J. Geophys. Res. 113, B06405. http://dx.doi.org/10.1029/2006JB004811.

Reasenberg, P.A., Simpson, R.W., 1992. Response of regional seismicity to the static stress change produced by the Loma Prieta earthquake. Science 255 (5052):1687–1690. http://dx.doi.org/10.1126/science.255.5052.1687.

Resende, R., Lamas, L.N., Lemos, J.V., Calçada, R., 2010. Micromechanical modelling of stress waves in rock and rock fractures. Rock Mech. Rock. Eng. 43 (6):741–761. http://dx.doi.org/10.1007/s00603-010-0098-1.

Ruch, J., Pepe, S., Casu, F., Solaro, G., Pepe, A., Acocella, V., Neri, M., Sansosti, E., 2013. Seismo-tectonic behavior of the Pernicana fault system (Mt Etna): a gauge for volcano flank instability? J. Geophys. Res. Solid Earth 118:4398–4409. http://dx.doi.org/10.1002/jgrb.50281.

Ryan, M.P., 1987. Neutral buoyancy and the mechanical evolution of magmatic systems, in magmatic processes: physicochemical principles, edited by B. O. Mysen. Spec. Publ. Geochem. Soc. 1, 259–288.

Ryan, M.P., 1993. Neutral buoyancy and the structure of mid-ocean ridge magma reservoirs. J. Geophys. Res. 98:22,321–22,338. http://dx.doi.org/10.1029/93JB02394.

Ryan, M.P., 1994. Neutral buoyancy-controlled magma transport and storage in mid-ocean ridge magma reservoirs and their sheeted dike complex: a summary of basic relationships. In: Ryan, M.P. (Ed.), Magmatic Systems. Academic, San Diego, Calif, pp. 97–135.

Sevilgen, V., Stein, R.S., Pollitz, F.F., 2012. Stress imparted by the great 2004 Sumatra earthquake shut down transforms and activated rifts up to 400 km away in the Andaman Sea. PNAS 109 (38):15152–15156. http://dx.doi.org/10.1073/pnas.1208799109.

Sheu, S.-Y., Shieh, C.F., 2004. Viscoelastic–afterslip concurrence: a possible mechanism in the early post-seismic deformation of the Mw 7.6, 1999 Chi-Chi (Taiwan) earthquake. Geophys. J. Int. 159:1112–1124. http://dx.doi.org/10.1111/j.1365-246X.2004.02437.x.

Singh, S.J., Rosenman, M., 1974. Quasi-static deformation of a viscoelastic half-space by a displacement dislocation. Phys. Earth Planet. Inter. 8:87–101. http://dx.doi.org/10.1016/0031-9201(74)90114-9.

Spampinato, L., Calvari, S., Oppenheimer, C., Lodato, L., 2008. Shallow magma transport for the 2002–3 Mt. Etna eruption inferred from thermal infrared surveys. J. Volcanol. Geotherm. Res. 177 (2):301–312. http://dx.doi.org/10.1016/j.jvolgeores.2008.05.013.

Steffke, A.M., Harris, A.J.L., Burton, M., Caltabiano, T., Salerno, G.G., 2011. Coupled use of COSPEC and satellite measurements to define the volumetric balance during effusive eruptions at Mt. Etna, Italy. J. Volcanol. Geotherm. Res. 205:47–53. http://dx.doi.org/10.1016/j.jvolgeores.2010.06.004.

Stein, R.S., 1999. The role of stress transfer in earthquake occurrence. Nature 402: 605–609. http://dx.doi.org/10.1038/45144.

Thatcher, W., Savage, J.C., 1982. Triggering of large earthquakes by magma-chamber inflation, Izu peninsula, Japan. Geology 10 (12):637–640. http://dx.doi.org/10.1130/0091-7613.

Toda, S., Stein, R.S., Sagiya, T., 2002. Evidence from the AD 2000 Izu islands earthquake swarm that stressing rate governs seismicity. Nature 419:58–61. http://dx.doi.org/10.1038/nature00997.

Toda, S., Stein, R.S., Lin, J., 2011. Widespread seismicity excitation throughout central Japan following the 2011 M = 9.0 Tohoku earthquake and its interpretation by Coulomb stress transfer. Geophys. Res. Lett. 38 (7). http://dx.doi.org/10.1029/2011GL047834.

Trasatti, E., Giunchi, C., Bonafede, M., 2003. Effects of topography and rheological layering on ground deformation in volcanic regions. J. Volcanol. Geotherm. Res. 122 (1–2): 89–110. http://dx.doi.org/10.1016/S0377-0273(02)00473-0.

Vidale, J., Agnew, D., Oppenheimer, D., Rodriquez, C., Houston, H., 1998. A weak correlation between earthquakes and extensional normal stress and stress rate from lunar tides. Eos Trans. AGU 79 (Fall Meet. Suppl., F641).

Walter, T.R., Amelung, F., 2004. Influence of volcanic activity at Mauna Loa, Hawaii, on earthquake occurrence in the Kaoiki Seismic Zone. Geophys. Res. Lett. 31, L07622. http://dx.doi.org/10.1029/2003GL019131.

Walter, T.R., Acocella, V., Neri, M., Amelung, F., 2005. Feedback processes between magmatic events and flank movement at Mount Etna (Italy) during the 2002–2003 eruption. J. Geophys. Res. 110, B10205. http://dx.doi.org/10.1029/2005JB003688.